Dual-Gated WTe 2 /MoSe 2 van der Waals Tandem Solar Cells

Nicolas Cavassilas, Demetrio Logoteta, Youseung Lee, Fabienne Michelini, Michel Lannoo, Marc Bescond, Mathieu Luisier

A Dual-Gated $WTe_2/MoSe_2$ van der Waals Tandem Solar Cell

Nicolas Cavassilas,*,† Demetrio Logoteta,† Youseung Lee,‡ Fabienne Michelini,† Michel Lannoo,† Marc Bescond,¶ and Mathieu Luisier§

†*Aix Marseille Université, CNRS, Université de Toulon, IM2NP UMR 7334, 13397, Marseille, France*

‡*Integrated Systems Laboratory, ETH Zürich, 8092 Zürich, Switzerland*

¶*LIMMS, CNRS-Institute of Industrial Science, UMI 2820, University of Tokyo, 153-8505 Tokyo, Japan*

§*Integrated Systems Laboratory, ETH Zürich, 5 PDF Rendering Error Something went wrong while rendering this PDF. 8092 Zürich, Switzerland*

E-mail: nicolas.cavassilas@im2np.fr

Abstract

We propose and numerically investigate, through a multi-scale approach, a tandem solar cell based on a van der Waals heterostructure composed of two monolayers of transition metal dichalcogenides. The electronic connection between the two subcells is obtained *via* tunneling through the van der Waals heterojunction which is electrostatically controlled by means of a dual-gate. Furthermore, by adjusting the dual-gate voltages, the photocurrents in the two subcells can be matched and the tandem cell performances optimized. Assuming an optimal absorptance, as expected in light-trapping systems, we predict that a power conversion efficiency of 30.7%, largely exceeding that of the single subcells, can be achieved. The proposed design being suitable for other

van der Waals heterojunctions, this result shows that it represents a viable option for future high efficiency photovoltaic.

Introduction

Next-generation photovoltaic devices are demanded to combine high efficiency with low-cost fabrication. Mechanical strength and flexibility are also important requisites. Monolayers of transition metal dichalcogenides (TMDs) such as MoS_2, $MoSe_2$, WSe_2 and WS_2, appear as promising building blocks to realize solar cells able to meet all these requirements.[1,2] Indeed, two-dimensional (2D) TMDs can be easily exfoliated from their earth-abundant bulk form, in which adjacent layers are held together by weak van der Waals interactions. The strong intra-layer covalent bonding, on the other hand, provides them with superior bendability and elasticity.[3] 2D TMDs are particularly well-suited for optoelectronics since they are direct-band gap semiconductors and, despite their atomic thickness, exhibit a significant optical absorption.[4] According to recent studies, their absorptance can be further increased up to an almost perfect level[5,6] by means of light trapping systems.[7] Besides, due to it extreme thinness, their optical properties can be tuned *via* doping, strain engineering or electrical gating.[8] **On the other hand, engineering the dielectric environment surrounding the 2D layers could be an effective way to reduce the exciton binding energies,[9] particularly large in 2D materials due to the weak dielectric screening.** Finally, owing to the absence of dangling bonds, they offer the opportunity to create all kinds of heterostructure configurations, regardless of lattice mismatch.[10,11]

TMD-based solar cells have been proposed both as planar[2,12–15] and vertical[16–19] homo-junctions/heterojunctions. In the planar configuration, a *p*-*n* junction providing the spatial electron-hole separation is generated by electrostatically doping the monolayers, or naturally results from the built-in electric field at the heterointerface. The efficiency of these cells is mainly limited by the absorption-collection trade-off between the size of the active area and

the strength of the electric field enabling the carrier separation.

In solar cells based on vertical heterojunctions of TMDs, the photovoltaic effect is mainly driven by spontaneous exciton dissociation induced by the type II band alignment.[19] In these devices, the efficiency is limited by the interlayer recombination of the photogenerated excitons. The latter is significant in the presence of large band offsets, which are nevertheless required to maintain a high electron/hole spatial separation. This interlayer recombination might partly explain why the open-circuit voltage V_{oc} is particularly low in comparison with the absorption band gaps.[16,18]

Despite the exciting opportunities offered by TMD-based solar cells, the above-mentioned architectures are still subject to the same fundamental limitations as single-junction cells relying on bulk structures. Their power conversion efficiency (PCE), in particular, cannot exceed the Schokley-Queisser limit of 33%.[20] Currently, multi-junction cells represent the only effective solution to overcome this limit, a five-junction cell holding the record performance with a PCE of 46% at 508 suns.[21] Other design options, including intermediate-band[22,23] and hot-carrier cells,[24] have been proposed but still fail at the device demonstration level. In a multi-junction cell, several single-junction subcells are vertically stacked in descending order of their band gap energy. The upper subcells automatically filter out high energy photons from the light spectrum that illuminates the underlying lower band gap subcells. This arrangement allows for the exploitation of a larger part of the solar spectrum and a simultaneous reduction of thermal losses. In practice, the fabrication is complicated by the limited choice of material combinations due to the lattice matching constraint, and by the need to interpose supplementary layers between the subcells to form low-resistance interconnections. The latter are realized as p-n band-to-band tunnel junctions which require high doping gradients to attain the required transparency. Furthermore carrier transport through these structures is often dominated by the presence of impurities and dislocations.

In this paper, we propose and discuss the performance of an original concept of tandem solar cell based on a hybrid planar-vertical configuration of 2D TMDs. In addition to the

low cost, such devices offer critical advantages over bulk multi-junction solar cells, in terms of relaxation of design constraints and optimization opportunities.

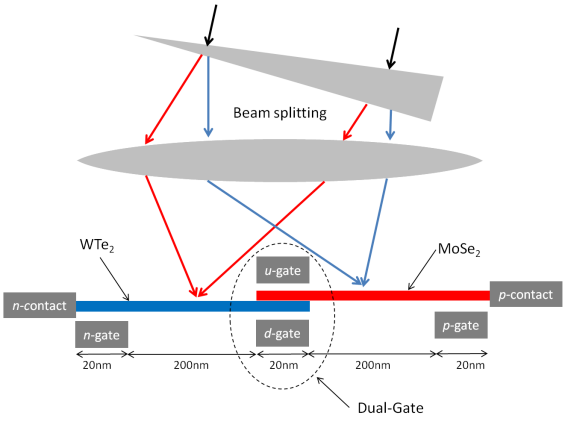

Figure 1: Schematic representation of the considered system including the proposed tandem solar cell. The WTe_2 and $MoSe_2$ subcells are connected *via* a heterojunction enclosed in a dual-gate system (u- and d-gates). The cell is contacted through the electrodes denoted as n- and p-contacts, while the purpose of the n- and p-gates is to electrostatically doped the layers. Note that the total length of this planar solar cell is limited by our computational resources, but in practice monolayers with lengths of the order of microns have been experimentally demonstrated.[2,12]

Method

The considered photovoltaic system including the tandem cell is schematically represented in Fig. 1. The cell consists of a 240nm long monolayer of WTe_2, acting as small-gap material ($E_g = 0.93$ eV). It partially overlaps with a monolayer of $MoSe_2$ of the same length, which plays the role of wide-gap material ($E_g = 1.67$ eV). A low-resistance connection between the layers is established by enforcing a suitable voltage at the central dual-gate (u- and d-gates) that can turn the band alignment of the 20nm long $WTe_2/MoSe_2$ heterojunction from type II to type III.[25,26] Under these conditions, the interlayer tunneling is strongly enhanced and the transfer of carriers from one layer to the other becomes significant, as the tunneling distance only amounts to the van der Waals gap.[25,27] The purpose of the 20 nm long n- and p-gates is to create an electrostatic doping close to the two contacts, n-type for WTe_2 and

p-type for $MoSe_2$. We assume that these gates are held at a fixed voltage, corresponding to an induced electrostatic doping of 3×10^{13} cm^{-2}. All the gate electrodes are separated from WTe_2 and $MoSe_2$ by a 3nm thick HfO_2 layer with a relative dielectric constant ϵ_r=20.

As mentioned before, the vertical structure of bulk multi-junction solar cells allows for an approximate matching between the band gap of a subcell and the energy of photons impinging over it. In the proposed tandem cell, this effect can be obtained by means of a spectral beam splitting system that deflects toward the WTe_2 and $MoSe_2$ monolayers photons with energy below and above the $MoSe_2$ band gap, respectively[7] (see Fig. 1). In order to increase the absorptance of the monolayers, the cell can be further embedded in a light-trapping microcavity, which, combined with a spectrum-splitting system, has been theoretically shown to enable over 90% light absorptance.[6]

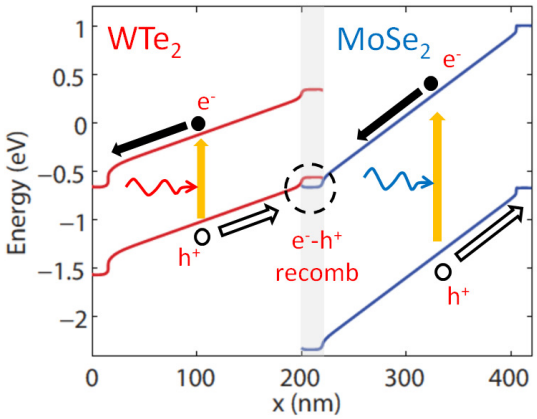

Figure 2: Calculated band diagram of the tandem solar cell along the transport direction under dark condition for $V = 0$ V, $V_u = 0.6$ V and $V_d = -0.6$ V. The region over which the monolayers overlap corresponds to the grey stripe. The operation of the device is also schematically illustrated.

Results

The calculated band diagram along the transport direction under dark condition, with zero voltage between the n- and p-contacts ($V = 0$ V), and voltages V_u=0.6 V and V_d=-0.6 V applied to the u- and d-gates of the dual-gate, respectively, is shown in Fig. 2. It was

obtained by means of a self-consistent atomistic full quantum simulations, calibrated on an *ab-initio* description of the structure depicted in Fig. 1 (see the Supporting Information (SI) for the details).

The operation of the device is also schematically illustrated in Fig. 2. The photogenerated electrons in WTe_2 and holes in $MoSe_2$ drift under the electric field toward the n- and p-contacts, respectively, while the corresponding holes in WTe_2 and electrons in $MoSe_2$ move toward the gated overlap region. According to the band diagram, the voltage difference $V_u - V_d = 1.2$ V opens an interlayer tunneling window of $\simeq 0.1$ eV by pushing the $MoSe_2$ conduction band below the WTe_2 valence band. Such a band-to-band tunneling junction, already experimentally demonstrated,[25] allows for electron-hole recombination and ensures the continuity of the current in the whole structure. **Moreover, according to Ref.,[9] the immediate proximity of the high-k dielectric and the metal gates is also expected to favor the dissociation of excitons possibly diffusing to this dual-gate.**

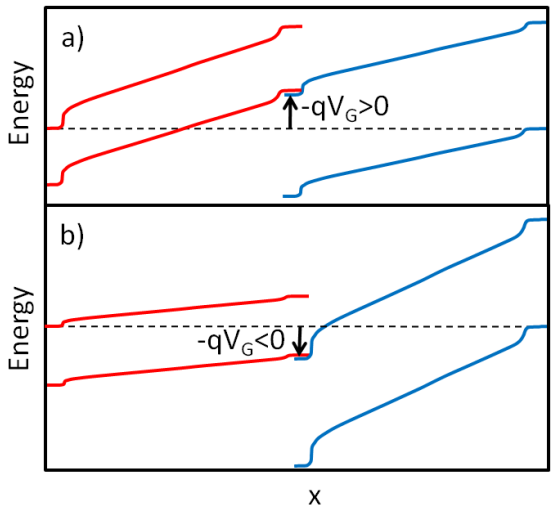

Figure 3: Schematic representation of the band diagram modification induced by the average bias V_G applied to the dual-gate. (a) A positive V_G increases the electric field in WTe_2 and simultaneously reduces it in $MoSe_2$ while (b) a negative V_G implies the opposite behavior.

In Fig. 2 the average voltage applied to the dual-gate is $V_G = (V_u + V_d)/2 = 0$. As illustrated in Fig. 3, a change of this voltage modifies the electric field in the ungated region of the monolayers. Particularly, the variations of the electric field in the two subcells are

opposite i.e. if the electric field increases in the WTe_2 subcell, it decreases in the $MoSe_2$ one, and *vice versa*. Thus, from a design perspective, the presence of the dual-gate introduces additional degrees of freedom, which can be exploited to match the photocurrents of the two subcells. This advantage, together with both opportunities to assume lattice mismatched heterojunctions and to control the tunnel junction, suggest high potentialities for the proposed device. The expected low fabrication cost represents a further remarkable benefit.

In the following, we evaluate the maximum performance that can be achieved by the tandem cell. We first calculate the photo-current independently in the WTe_2 and $MoSe_2$ subcells without considering the van der Waals connection. For this purpose we resort the semi-classical one-dimensional drift-diffusion solver implemented in the SCAPS simulation package.[28] Such an approach, which is described in the SI appears well-suited for the problem under consideration as no quantum effects are expected to affect the in-plane transport of both layers. We assume photogeneration rates corresponding to an illumination of 1 sun and to the high broadband absorptance attainable by embedding the cells in a wedge-shaped microcavity.[6]

The current-voltage characteristics of the two subcells are reported in Fig. 4(a). Due to the narrower band gap, the WTe_2 subcell exhibits a larger short-circuit current with respect to the $MoSe_2$ counterpart. On the other hand, the roughly linear dependence of the open-circuit voltage on the band gap entails that the WTe_2 cell has a significantly smaller V_{oc} (0.40 V *vs* 1.15 V for $MoSe_2$), and, overall, a smaller PCE (17.5% *vs* 23.0% for $MoSe_2$). In order to take into account the filtering action of the spectral beam splitting system (see Fig. 1), in the following we will consider the current-voltage characteristic of the WTe_2 subcell obtained by cutting off the solar spectrum components at energies higher than the $MoSe_2$ band gap (see Fig. 4(a)). We will refer to the current-voltage characteristic of the WTe_2 (filtered) and $MoSe_2$ subcells, as $J_{WTe_2}(V_{WTe_2})$ and $J_{MoSe_2}(V_{MoSe_2})$, respectively.

The tandem cell is modeled as the series of the WTe_2 and $MoSe_2$ subcells, interconnected

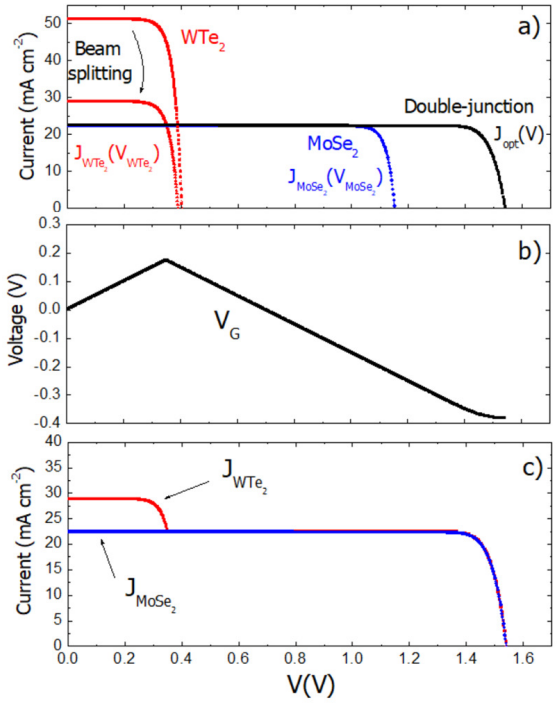

Figure 4: (a) Current-voltage characteristics of the WTe_2 and $MoSe_2$ uncoupled subcells, computed with SCAPS, and of the optimized tandem cell. The curve denoted by $J_{MoSe_2}(V_{MoSe_2})$ is the current in the $MoSe_2$ subcell, while that denoted by $J_{WTe_2}(V_{WTe_2})$ is the current in the WTe_2 cell once the photons with energy larger than 1.67eV (energy gap of $MoSe_2$) are filtered. This latter curve therefore represents the current in the WTe_2 cell under the beam splitting system. The curve denoted $J_{opt}(V)$ refers to the optimized tandem solar cell. Corresponding (b) average voltage V_G applied to the dual-gate and (c) currents of the WTe_2 and $MoSe_2$ subcells.

through a perfectly transmitting tunnel junction. The photocurrent J flowing through the cell is thus limited to the smallest current flowing in the single subcells. As mentioned before, at each V the performance of the tandem cell can be optimized by tuning V_G. The corresponding optimized current-voltage characteristic $J_{opt}(V)$ is reported in Fig. 4(a) (see the SI for the calculation details). The corresponding values of V_G and of J_{WTe_2} and J_{MoSe_2}, are shown in Figs. 4(b) and 4(c), respectively. At low V, $J_{WTe_2} > J_{MoSe_2}$ and therefore $J_{opt} = J_{MoSe_2}$. The excess carriers photogenerated in the WTe_2 subcell are lost by recombination. For high V, up to V_{oc}, V_G is adjusted so that J_{WTe_2} and J_{MoSe_2} remain equal. This result, shown in Fig. 4(c), confirms that the best tandem cell is obtained when the currents in both subcells are equal.

From the curve $J_{\rm opt}(V)$ we can extract V_{oc}, the fill factor and the PCE. Thanks to the adjustable V_G, with V_{oc}=1.54 V, we are very close to the maximum achievable value, i.e. 1.55 V for the sum of the V_{oc}'s from each single subcells. Moreover, we obtain an optimal fill factor of 0.89 *vs* 0.85 and 0.89 respectively for WTe_2 and $MoSe_2$. The maximum power is obtained at $V = 1.41$ V, resulting in a PCE as high as 30.7%. Finally, to highlight the importance of properly adjusting V_G, we mention that V_{oc} and PCE strongly decrease to 0.78V and 15.6%, respectively, if we keep $V_G = 0$ V in our simulations.

Conclusion

In conclusion, we have proposed a tandem solar cell based on 2D TMDs. The interconnection between the monolayers constituting the two subcells is implemented by electrostatically inducing an interlayer tunneling window through a van der Waals heterojunction *via* a dual-gate. Selecting the dual-gate voltages also provides a way to tune the electric field within the absorption area, which can be exploited to match the photocurrents in the subcells. We show that such a design leads to an excellent combination of the two subcells with open-circuit voltage and fill factor both very close to the best achievable. This additional degree of freedom, together with the poor sensitivity to the lattice mismatch and low cost fabrications, translate into unique advantages with respect to bulk multi-junction cells. In the presence of a photonic system allowing for efficient absorption, our simulations predict a PCE of 30.7%, much higher than any competing technology with such tiny dimensions. **Although this result should be tempered by the technological challenge associated with the fabrication of the auxiliary light trapping system, we point out that by replacing this system with a simple back mirror, a still promising PCE of 5.86%, against 2.76% and 4.38% for the WTe_2 and $MoSe_2$ single subcells, respectively, is obtained. Overall, our calculations clearly indicate that gated van der Waals heterojunctions of TMDs represent a viable option for future efficient**

photovoltaics.

Supporting Information

Details of the models use in this theoretical investigations. Parameters injected in the semi-classical model.

Acknowledgement

MB acknowledges the PEPS Project ICE from Réseaux Ingénierie verte of the CNRS. YL and ML acknowledge funding by the MARVEL National Centre of Competence in Research of the Swiss National Science Foundation and by ETH Zürich under Grant ETH-32 15-1.

References

(1) Das, S.; Pandey, D.; Thomas, J.; Roy, T. The Role of Graphene and Other 2D Materials in Solar Photovoltaics. *Advanced Materials* **2018**, 1802722.

(2) Pospischil, A.; Furchi, M. M.; Mueller, T. Solar-energy conversion and light emission in an atomic monolayer pn diode. *Nature Nanotechnology* **2014**, *9*, 257–261.

(3) Akinwande, D.; Petrone, N.; Hone, J. Two-dimensional flexible nanoelectronics. *Nature Communications* **2014**, *5*.

(4) Bernardi, M.; Palummo, M.; Grossman, J. C. Extraordinary Sunlight Absorption and One Nanometer Thick Photovoltaics Using Two-Dimensional Monolayer Materials. *Nano Letters* **2013**, *13*, 3664–3670.

(5) Jiang, X.; Wang, T.; Xiao, S.; Yan, X.; Cheng, L.; Zhong, Q. Approaching perfect absorption of monolayer molybdenum disulfide at visible wavelengths using critical coupling. *arXiv:1802.00586 [physics]* **2018**, arXiv: 1802.00586.

(6) Wu, Y.-B.; Yang, W.; Wang, T.-B.; Deng, X.-H.; Liu, J.-T. Broadband perfect light trapping in the thinnest monolayer graphene-MoS2 photovoltaic cell: the new application of spectrum-splitting structure. *Scientific Reports* **2016**, *6*.

(7) Huang, Q.; Wang, J.; Quan, B.; Zhang, Q.; Zhang, D.; Li, D.; Meng, Q.; Pan, L.; Wang, Y.; Yang, G. Design and fabrication of a diffractive optical element as a spectrum-splitting solar concentrator for lateral multijunction solar cells. *Applied Optics* **2013**, *52*, 2312.

(8) Wang, Q. H.; Kalantar-Zadeh, K.; Kis, A.; Coleman, J. N.; Strano, M. S. Electronics and optoelectronics of two-dimensional transition metal dichalcogenides. *Nature Nanotechnology* **2012**, *7*, 699–712.

(9) Latini, S.; Olsen, T.; Thygesen, K. S. Excitons in van der Waals heterostructures: The important role of dielectric screening. *Physical Review B* **2015**, *92*.

(10) Gong, C.; Zhang, H.; Wang, W.; Colombo, L.; Wallace, R. M.; Cho, K. Band alignment of two-dimensional transition metal dichalcogenides: Application in tunnel field effect transistors. *Applied Physics Letters* **2013**, *103*, 053513.

(11) Kang, J.; Tongay, S.; Zhou, J.; Li, J.; Wu, J. Band offsets and heterostructures of two-dimensional semiconductors. *Applied Physics Letters* **2013**, *102*, 012111.

(12) Baugher, B. W. H.; Churchill, H. O. H.; Yang, Y.; Jarillo-Herrero, P. Optoelectronic devices based on electrically tunable pn diodes in a monolayer dichalcogenide. *Nature Nanotechnology* **2014**, *9*, 262–267.

(13) Fontana, M.; Deppe, T.; Boyd, A. K.; Rinzan, M.; Liu, A. Y.; Paranjape, M.; Barbara, P. Electron-hole transport and photovoltaic effect in gated MoS2 Schottky junctions. *Scientific Reports* **2013**, *3*.

(14) Duan, X.; Wang, C.; Shaw, J. C.; Cheng, R.; Chen, Y.; Li, H.; Wu, X.; Tang, Y.; Zhang, Q.; Pan, A. et al. Lateral epitaxial growth of two-dimensional layered semiconductor heterojunctions. *Nature Nanotechnology* **2014**, *9*, 1024–1030.

(15) Li, M.-Y.; Shi, Y.; Cheng, C.-C.; Lu, L.-S.; Lin, Y.-C.; Tang, H.-L.; Tsai, M.-L.; Chu, C.-W.; Wei, K.-H.; He, J.-H. et al. Epitaxial growth of a monolayer WSe2-MoS2 lateral p-n junction with an atomically sharp interface. *Science* **2015**, *349*, 524–528.

(16) Furchi, M. M.; Zechmeister, A. A.; Hoeller, F.; Wachter, S.; Pospischil, A.; Mueller, T. Photovoltaics in Van der Waals Heterostructures. *IEEE Journal of Selected Topics in Quantum Electronics* **2017**, *23*, 106–116.

(17) Svatek, S. A.; Antolin, E.; Lin, D.-Y.; Frisenda, R.; Reuter, C.; Molina-Mendoza, A. J.;

Muoz, M.; Agrat, N.; Ko, T.-S.; de Lara, D. P. et al. Gate tunable photovoltaic effect in MoS $_2$ vertical pn homostructures. *Journal of Materials Chemistry C* **2017**, *5*, 854–861.

(18) Tsai, M.-L.; Su, S.-H.; Chang, J.-K.; Tsai, D.-S.; Chen, C.-H.; Wu, C.-I.; Li, L.-J.; Chen, L.-J.; He, J.-H. Monolayer MoS $_2$ Heterojunction Solar Cells. *ACS Nano* **2014**, *8*, 8317–8322.

(19) Lee, C.-H.; Lee, G.-H.; van der Zande, A. M.; Chen, W.; Li, Y.; Han, M.; Cui, X.; Arefe, G.; Nuckolls, C.; Heinz, T. F. et al. Atomically thin pn junctions with van der Waals heterointerfaces. *Nature Nanotechnology* **2014**, *9*, 676–681.

(20) Shockley, W.; Queisser, H. J. Detailed Balance Limit of Efficiency of *pn* Junction Solar Cells. *Journal of Applied Physics* **1961**, *32*, 510–519.

(21) Green, M. A.; Hishikawa, Y.; Warta, W.; Dunlop, E. D.; Levi, D. H.; Hohl-Ebinger, J.; Ho-Baillie, A. W. Solar cell efficiency tables (version 50). *Progress in Photovoltaics: Research and Applications* **2017**, *25*, 668–676.

(22) Luque, A.; Mart, A. Increasing the Efficiency of Ideal Solar Cells by Photon Induced Transitions at Intermediate Levels. *Physical Review Letters* **1997**, *78*, 5014–5017.

(23) Chen, S.-F.; Wu, Y.-R. A design of intermediate band solar cell for photon ratchet with multi-layer MoS $_2$ nanoribbons. *Applied Physics Letters* **2017**, *110*, 201109.

(24) Ross, R. T.; Nozik, A. J. Efficiency of hotcarrier solar energy converters. *Journal of Applied Physics* **1982**, *53*, 3813–3818.

(25) Roy, T.; Tosun, M.; Cao, X.; Fang, H.; Lien, D.-H.; Zhao, P.; Chen, Y.-Z.; Chueh, Y.-L.; Guo, J.; Javey, A. Dual-Gated MoS $_2$ /WSe $_2$ van der Waals Tunnel Diodes and Transistors. *ACS Nano* **2015**, *9*, 2071–2079.

(26) Cao, J.; Logoteta, D.; Ozkaya, S.; Biel, B.; Cresti, A.; Pala, M. G.; Esseni, D. Operation

and Design of van der Waals Tunnel Transistors: A 3-D Quantum Transport Study. *IEEE Transactions on Electron Devices* **2016**, *63*, 4388–4394.

(27) Szabo, A.; Koester, S. J.; Luisier, M. *Ab-Initio* Simulation of van der Waals $MoTe_2$ SnS_2 Heterotunneling FETs for Low-Power Electronics. *IEEE Electron Device Letters* **2015**, *36*, 514–516.

(28) Burgelman, M.; Nollet, P.; Degrave, S. Modelling polycrystalline semiconductor solar cells. *Thin Solid Films* **2000**, *361-362*, 527–532.

Graphical TOC Entry